Supporting Information

Electrochemical Biomass Valorization of Furfural to Maleic Acid by Modulating Selectivity with Bi-doped Lead Oxide

Eunchong Lee[a], Jae Hyung Kim[b], Juhyung Choi[a], Yewon Hong[a], Dongwoo Shin[a], Hyewon Yun[ac], Jimin Kim[ac], Gwangsu Bak[a], Seongin Hong[a] and Yun Jeong Hwang[*ac]

[a]Department of Chemistry, College of Natural Sciences, Seoul National University (SNU), Seoul 08826, Republic of Korea.

[b]Clean Fuel Research Laboratory, Korea Institute of Energy Research, Daejeon 34129, Republic of Korea.

[c]Center for Nanoparticle Research, Institute for Basic Science (IBS), Seoul 08826, Republic of Korea.

*e-mail: yjhwang1@snu.ac.kr

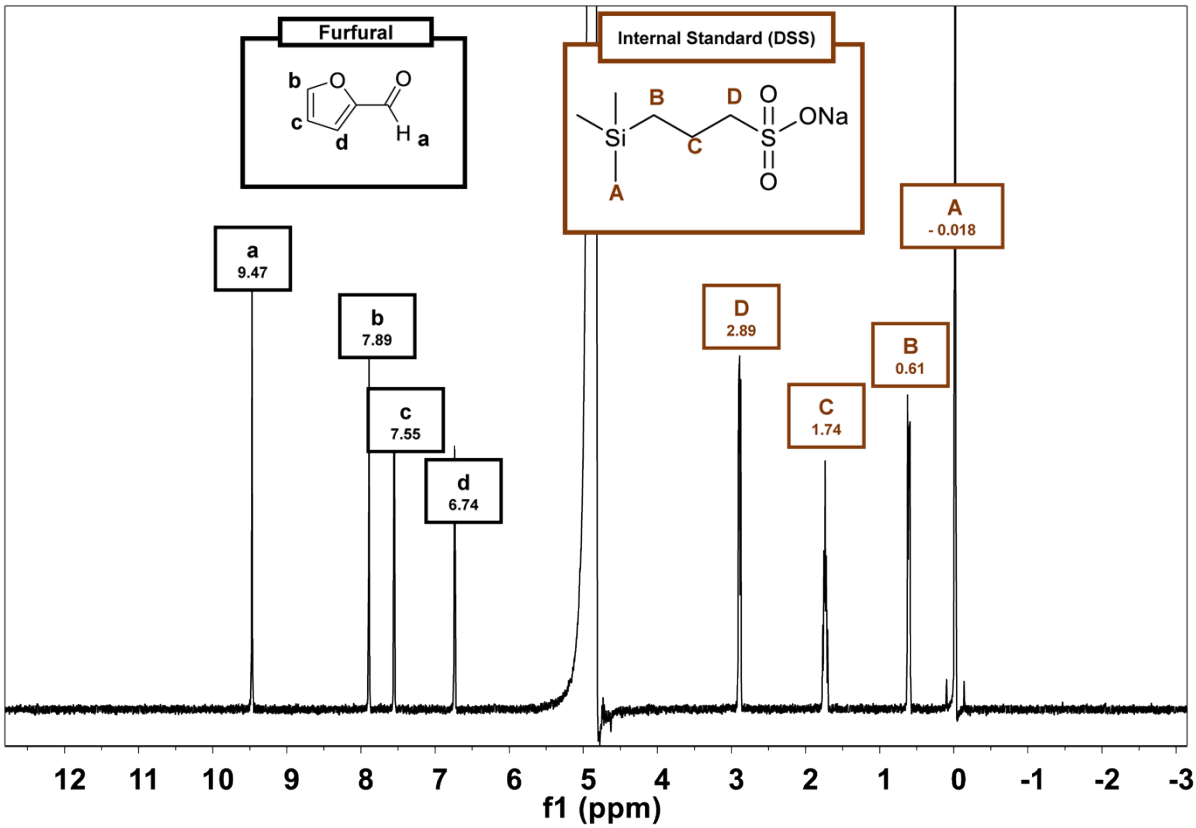

Fig. S1 NMR spectra of furfural

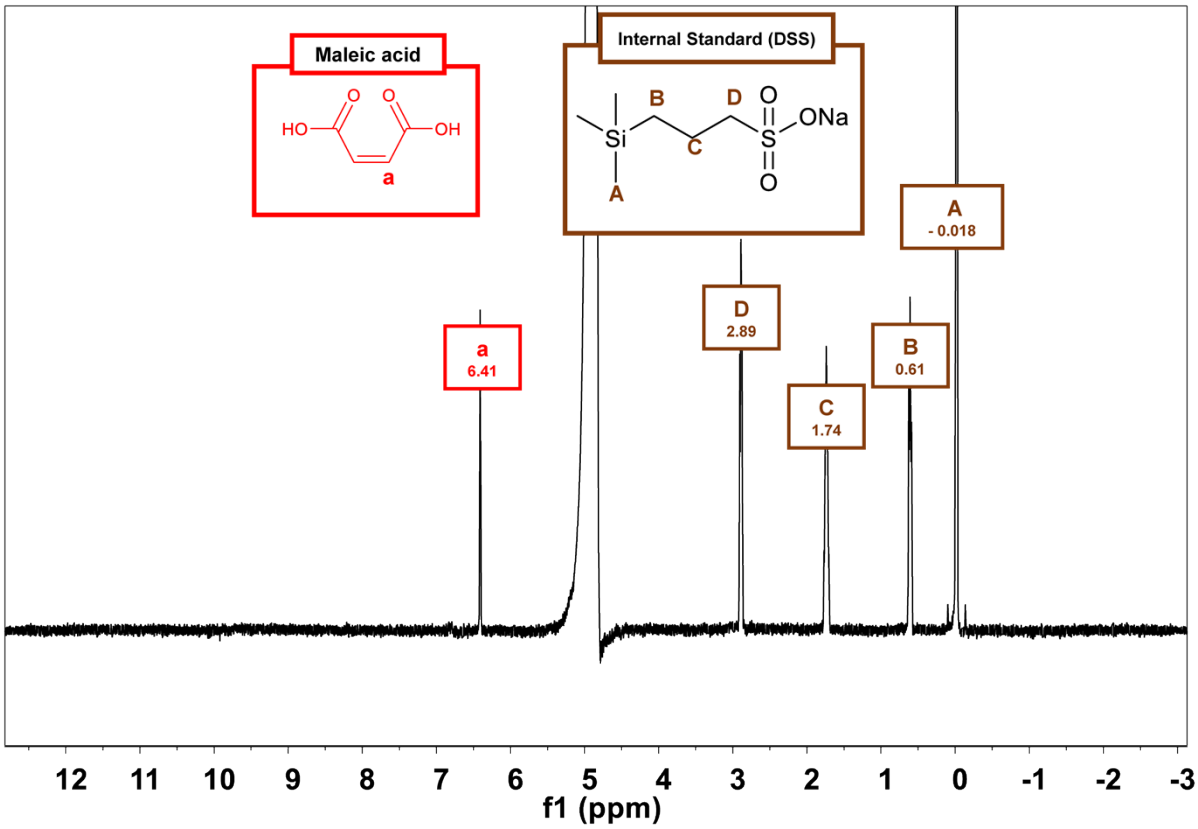

Fig. **S2** NMR spectra of maleic acid

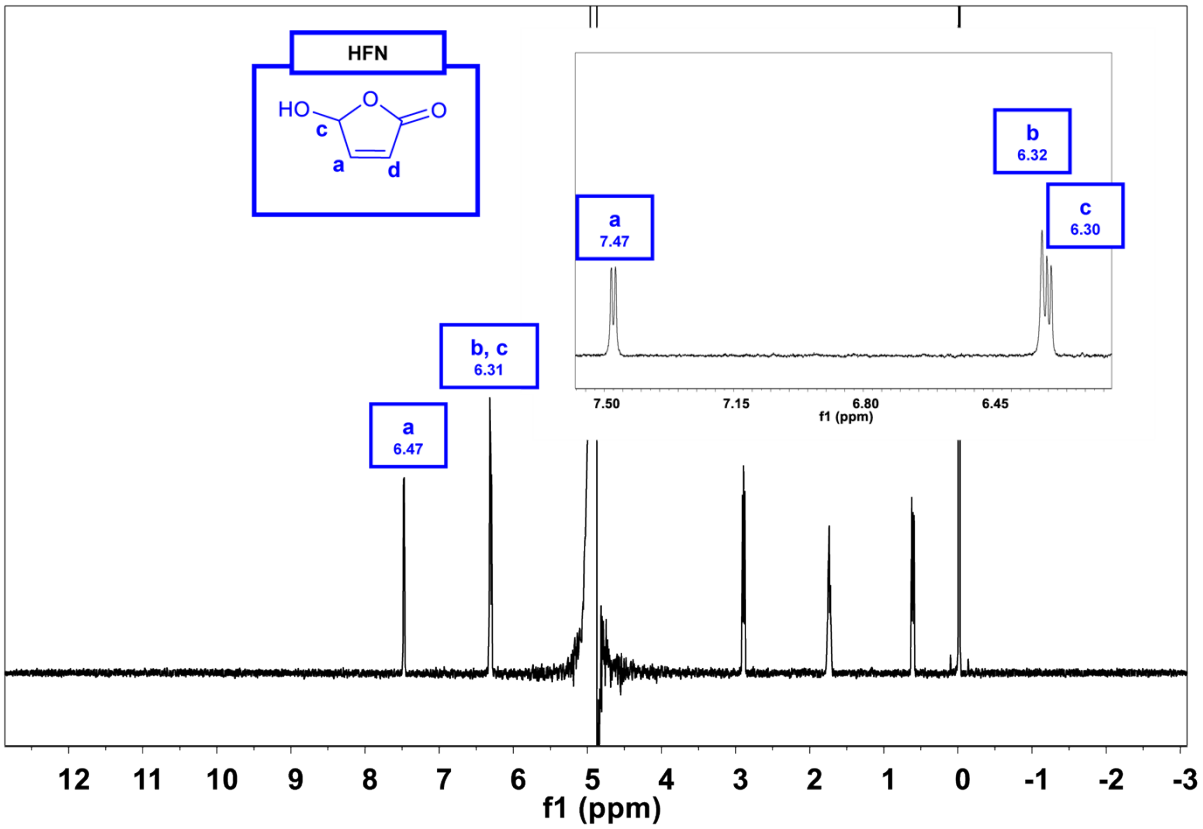

Fig. S3 NMR spectra of HFN

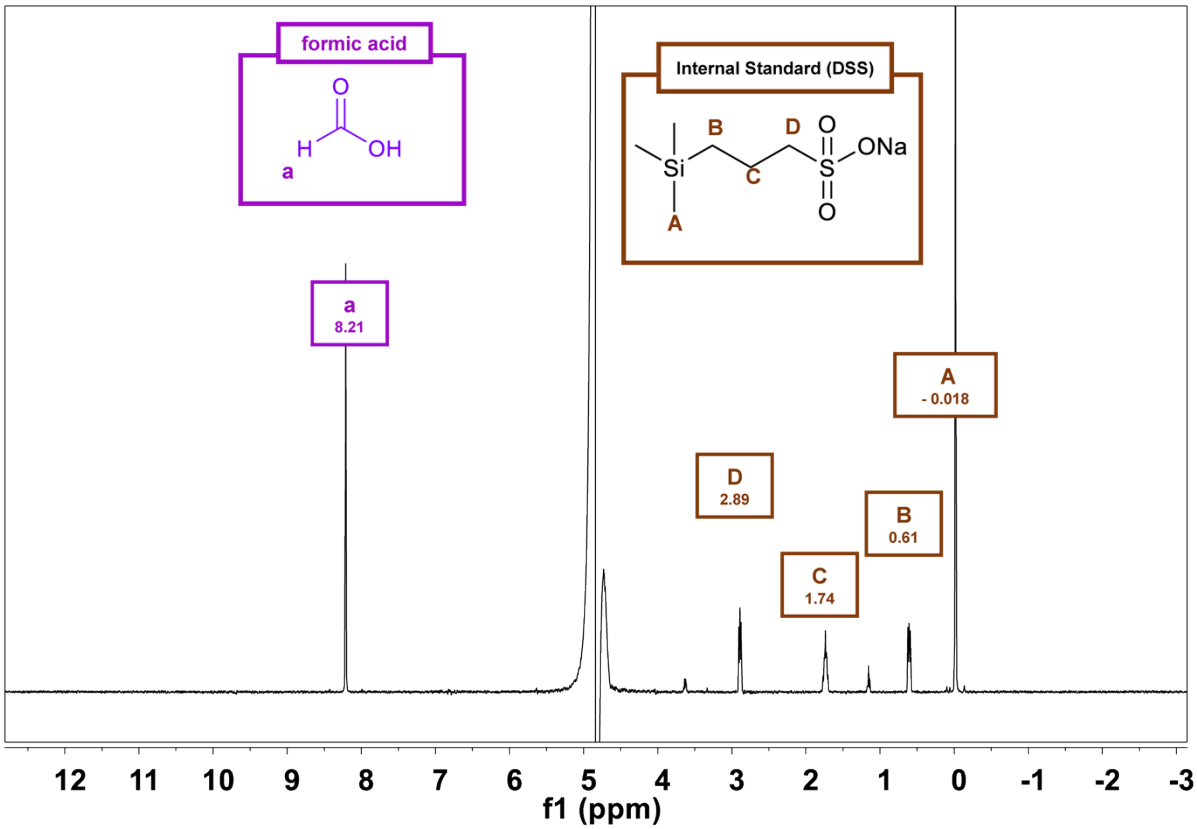

Fig. S4 NMR spectra of formic acid

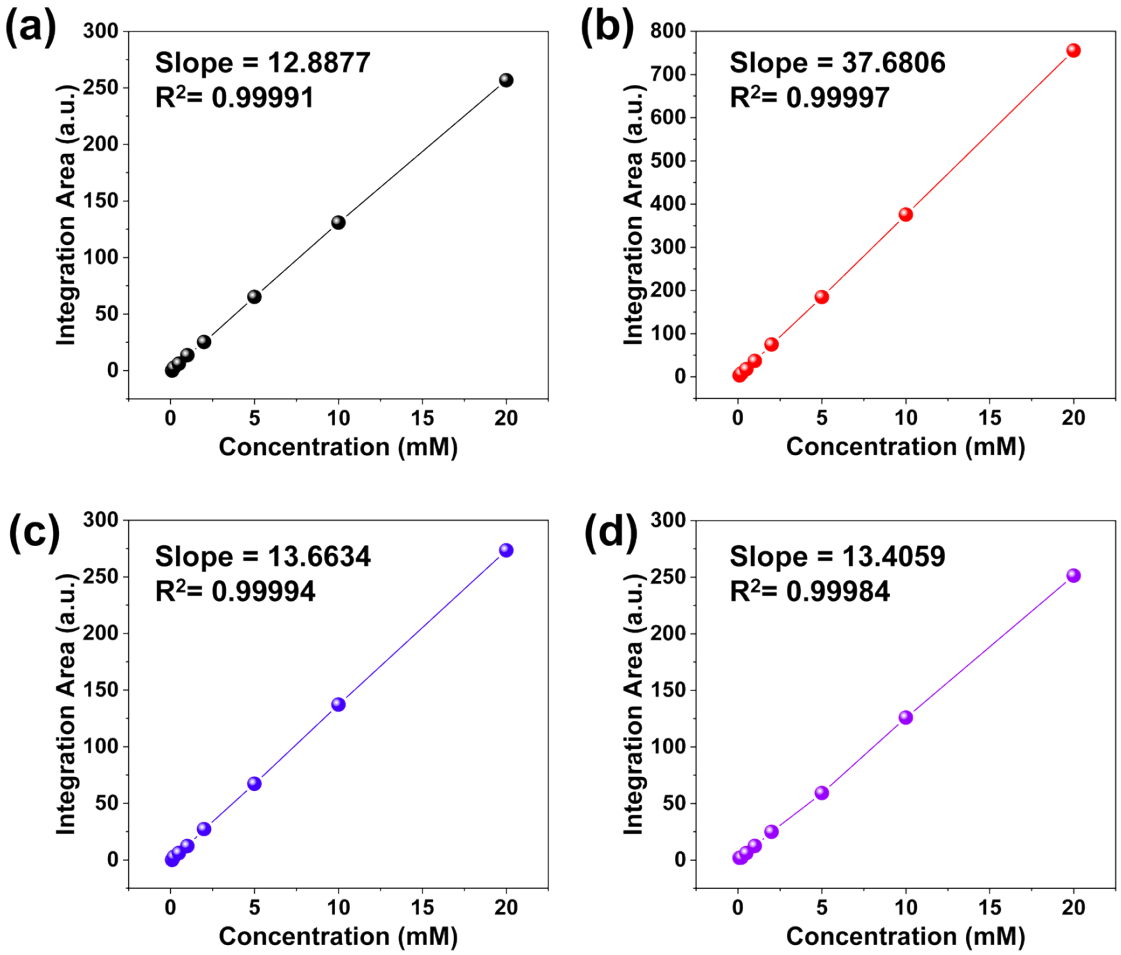

Fig. S5 NMR Calibration curves of (a) FF, (b) MA, (c) HFN, (d) FA

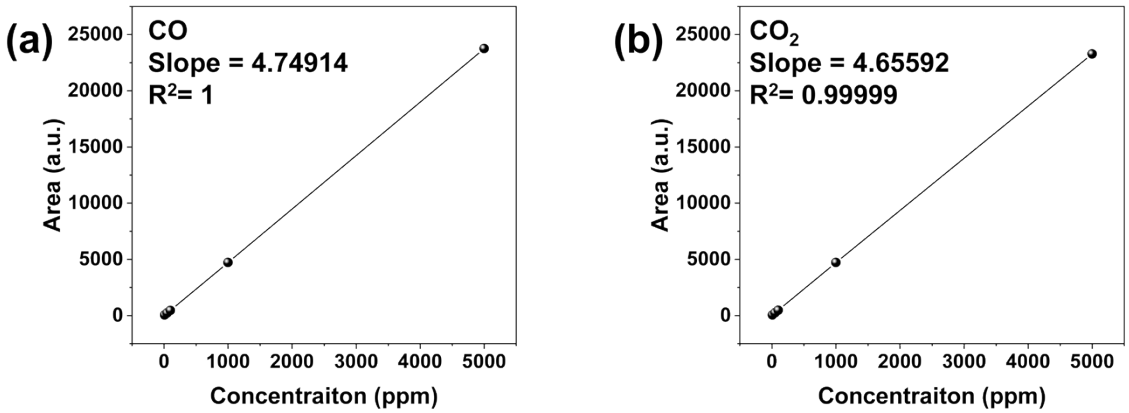

Fig. S6 Calibration Curves of (a) CO and (b) CO_2.

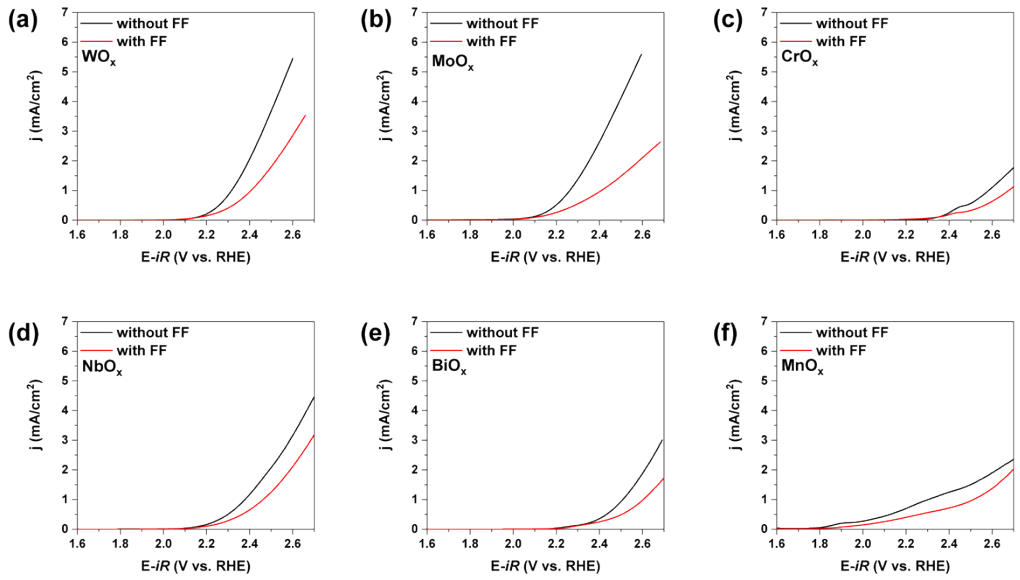

Fig. S7 LSV comparison without and with 10 mM FF in 0.1 M H_2SO_4 using various metal oxides at a scan rate of 5 mV/s/

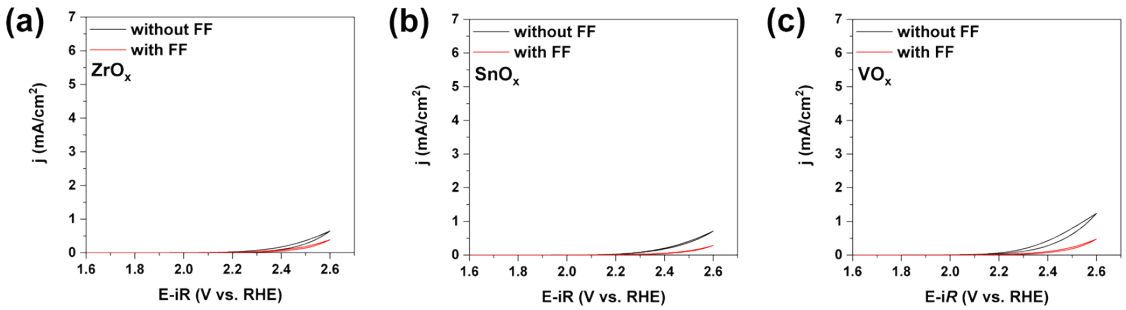

Fig. S8 CV comparison without and with 10 mM FF in 0.1 M H_2SO_4 using various metal oxides at a scan rate of 50 mV/s.

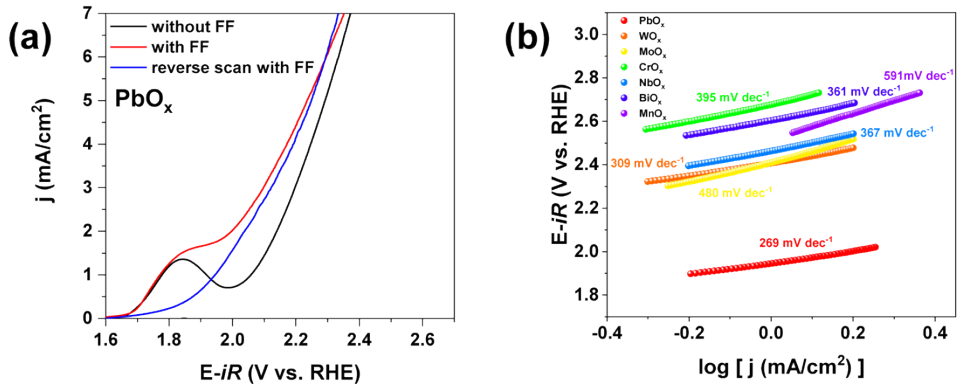

Fig. S9 (a) LSV curves of PbO_x without and with 10 mM FF in 0.1 M H_2SO_4 at a scan rate of 5 mV/s. (b) Tafel plot of FFOR condition using various metal oxides.

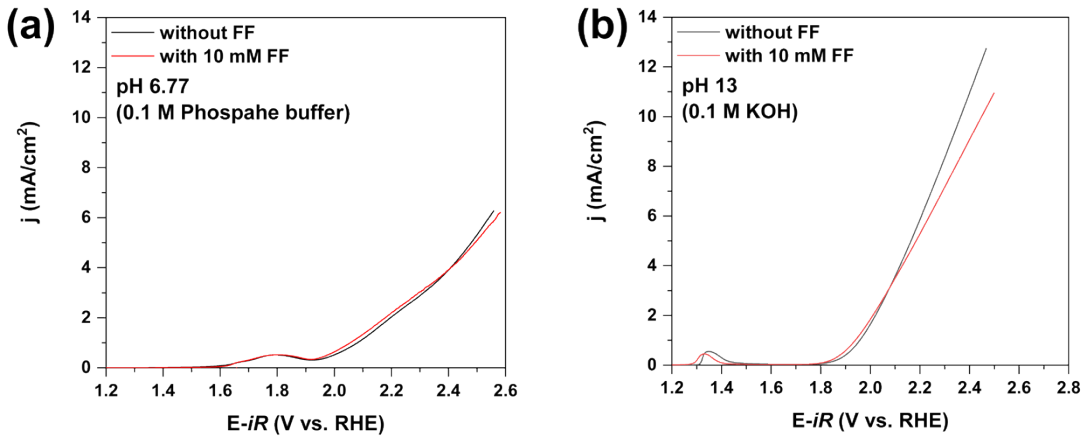

Fig. S10 LSV curves of PbO_x without and with 10 mM FF in (a) 0.1 M phosphate buffer ($NaHPO_4/Na_2PO_4$) and (b) 0.1 M KOH at a scan rate of 5 mV/s.

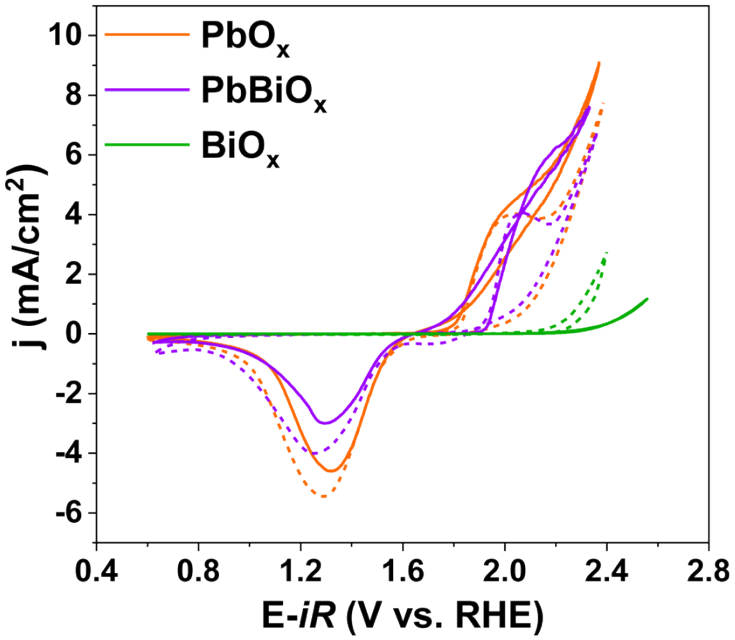

Fig. S11 CV curves comparison without/with 10 mM FF using PbO_x, $PbBiO_x$, and BiO_x at a scan rate of 20 mV/s. Dash lines are conducted without furfural in 0.1 M H_2SO_4. Straight lines are conducted with 10 mM FF in 0.1 M H_2SO_4.

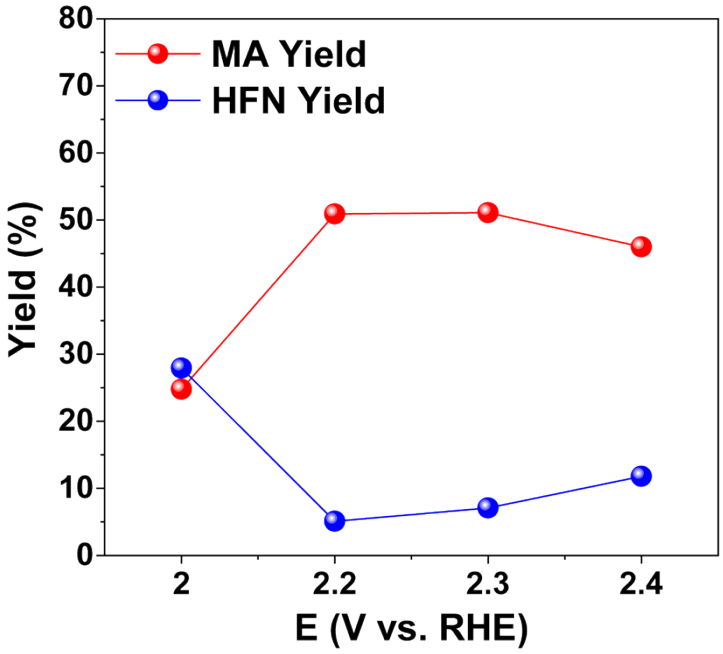

Fig. S12 Yield of MA and HFN using $PbBiO_x$ depending on the applied potential with 10 mM FF in 0.1 M H_2SO_4.

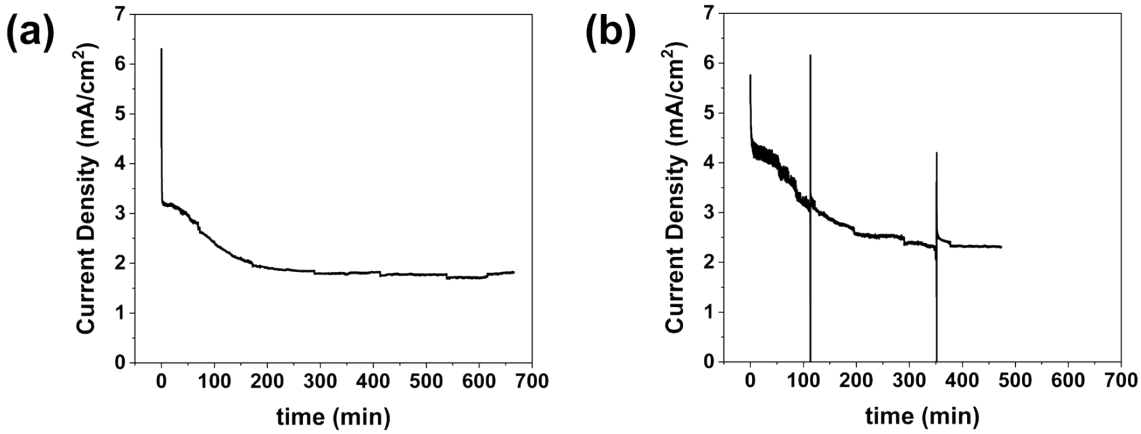

Fig. S13 CA curves in 0.1 M H_2SO_4 15 mL with 10 mM FF using (a) PbO_x and (b) $PbBiO_x$.

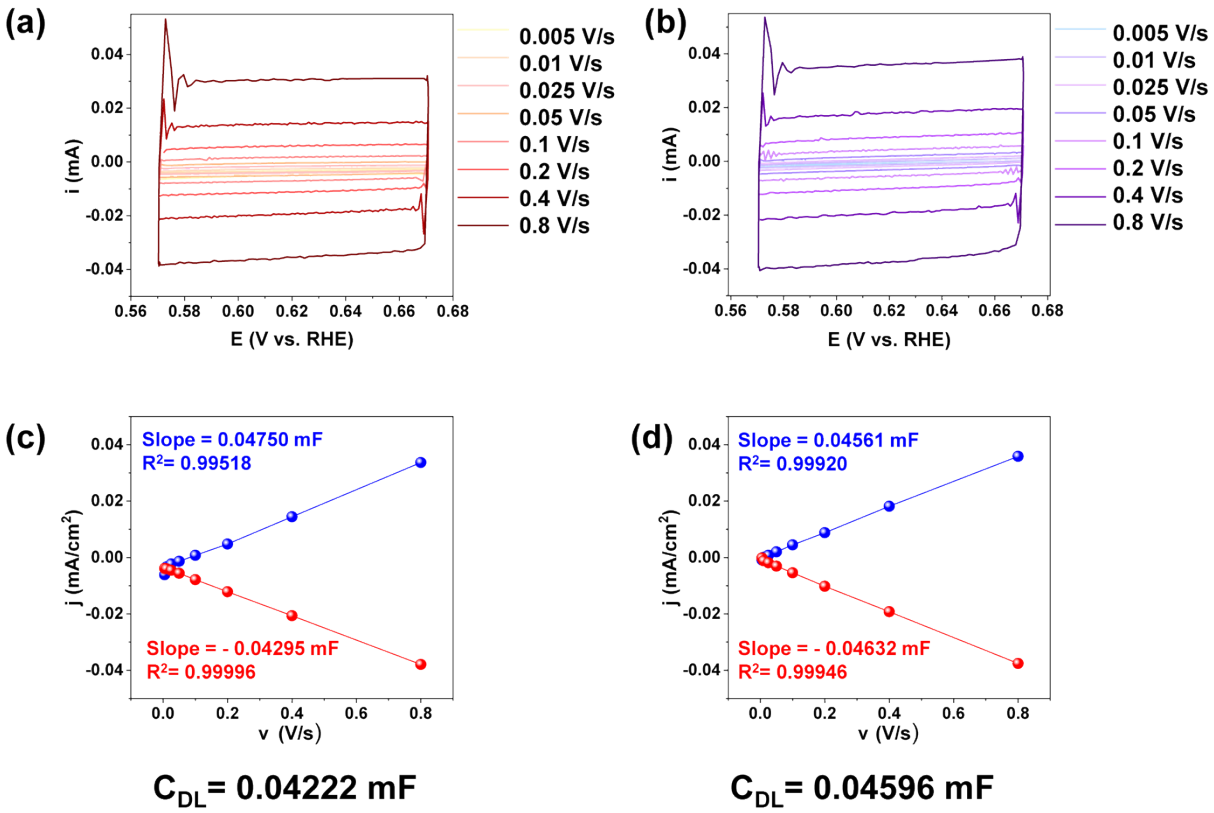

Fig. S14 Scan rate dependence of CVs of (a) PbO_x and (b) $PbBiO_x$. A plot of current versus scan rate to determine capacitance of (c) PbO_x and (d) $PbBiO_x$ with calculated C_{DL} values.

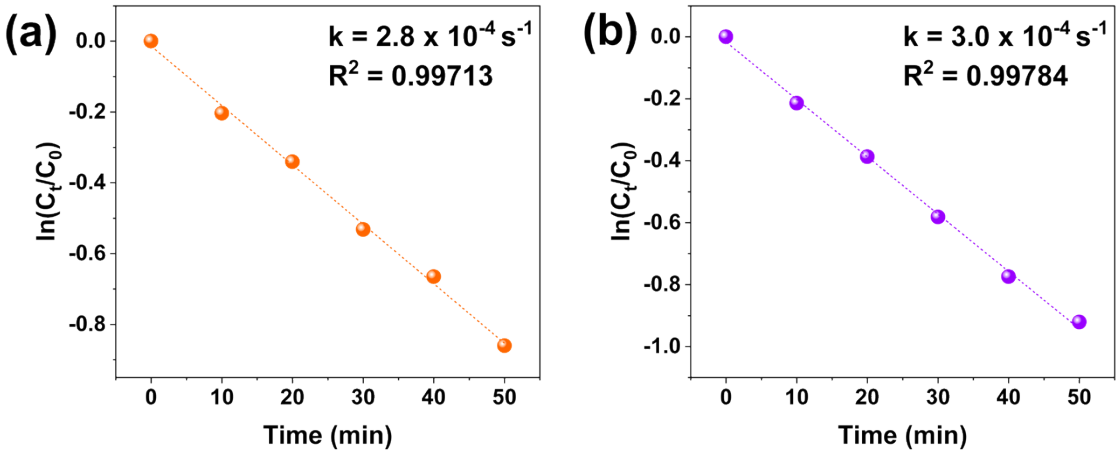

Fig. S15 Plot of concentration variation to time of (a) PbO_x, and (b) $PbBiO_x$ obtained during FFOR at 2.2 V vs. RHE with 10 mM FF. The plot showed the linearity of the log scale of concentration to time. the reaction order follows 1st order rate reaction.

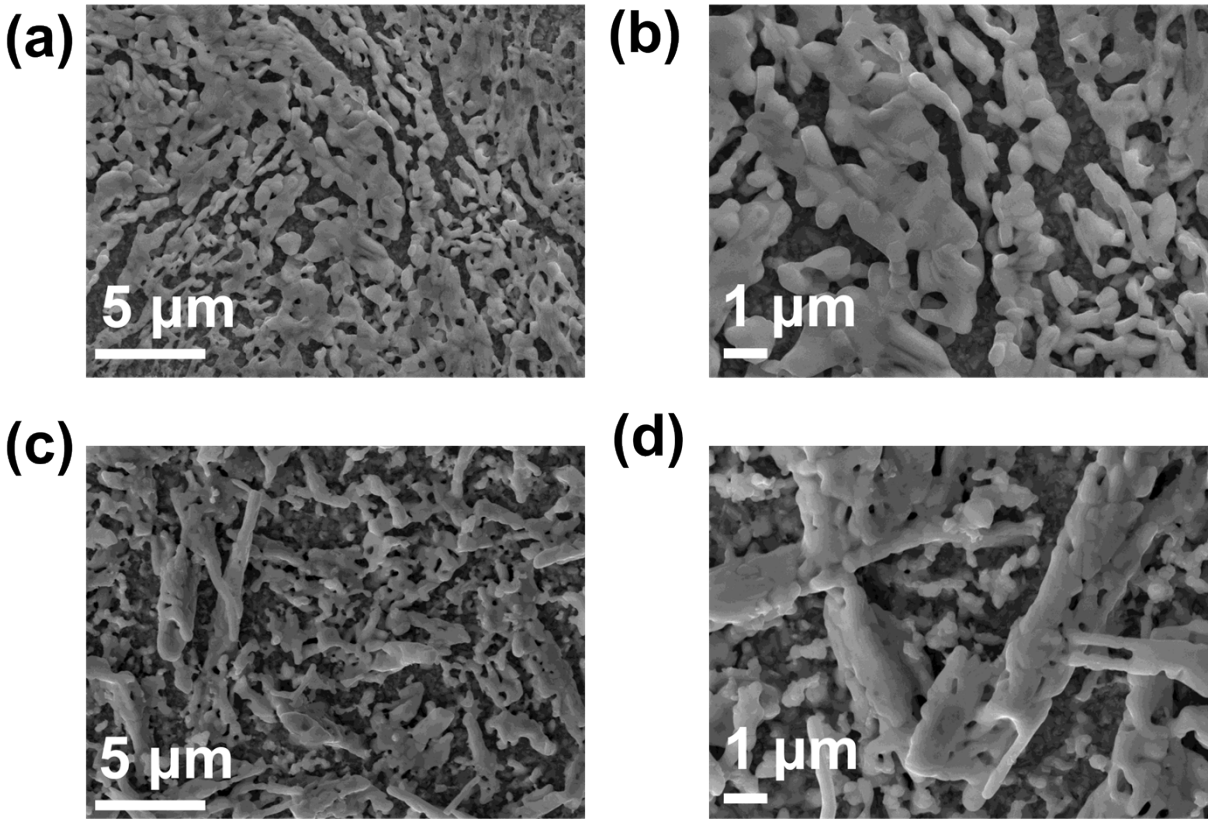

Fig. S16 (a) Low, and (b) high magnification SEM images of the as-prepared PbO_x before FFOR. (c) Low, and (d) high magnification SEM images of the as-prepared $PbBiO_x$ before FFOR.

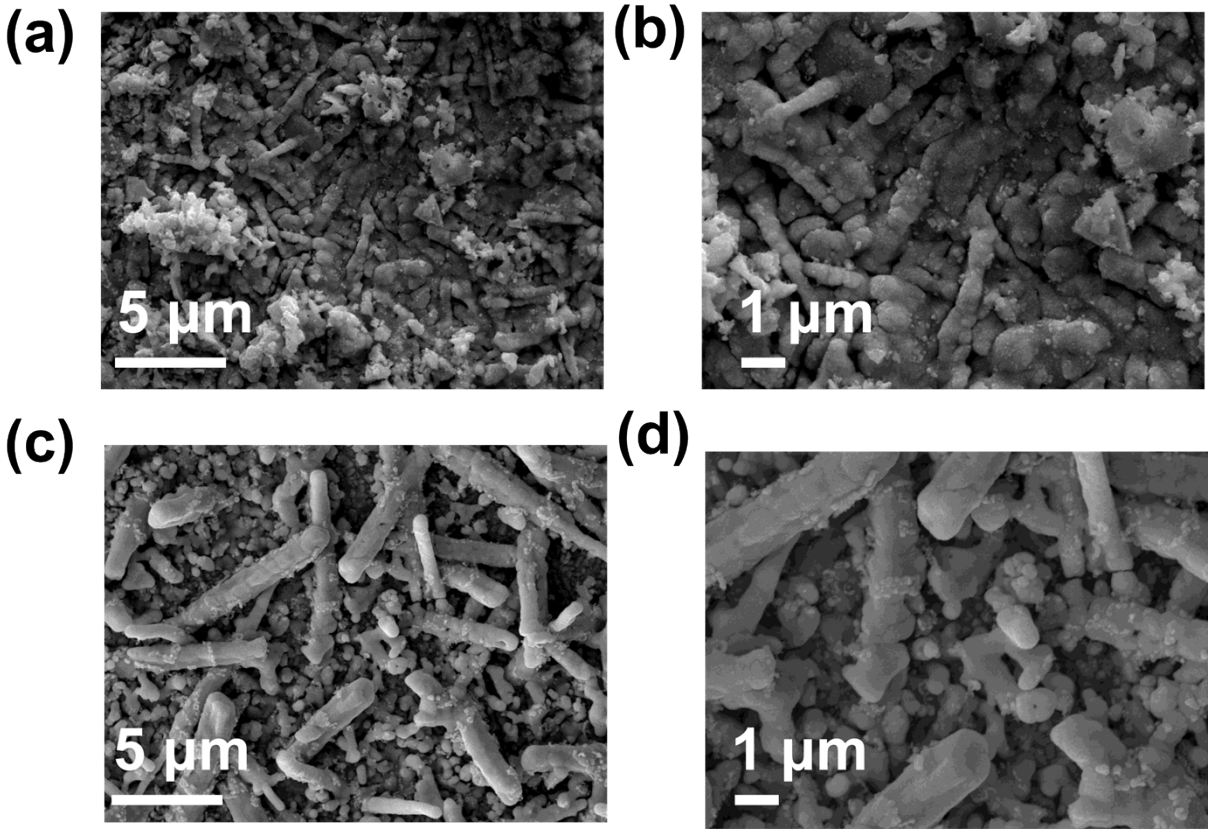

Fig. S17. (a) Low, and (b) high magnification SEM images of PbO_x anode after FFOR. (c) low, (d) high magnification SEM images of $PbBiO_x$ anode after FFOR.

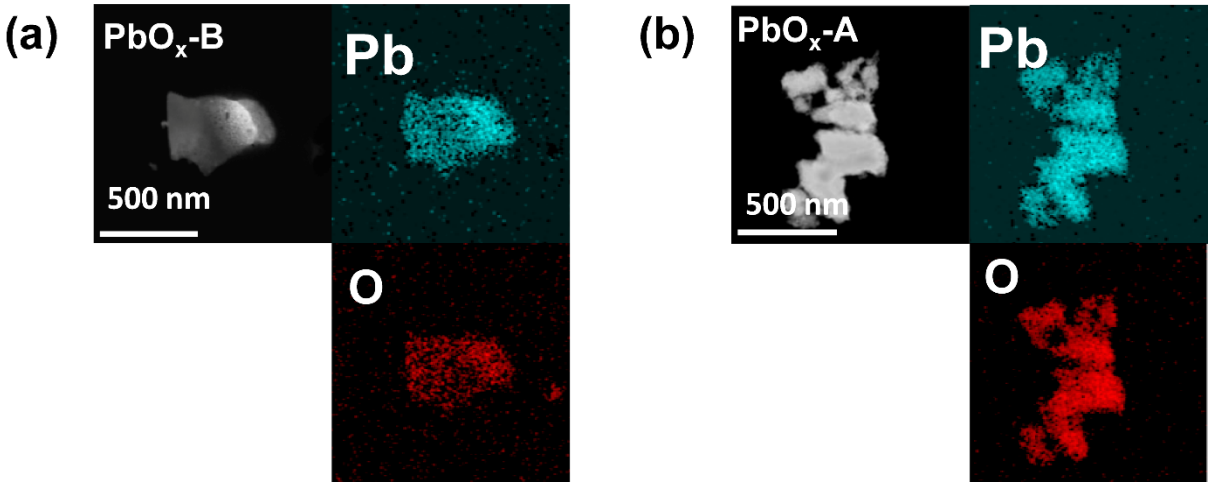

Fig. S18. STEM-EDS mappings of (a) PbO_x-B and (b) PbO_x-A.

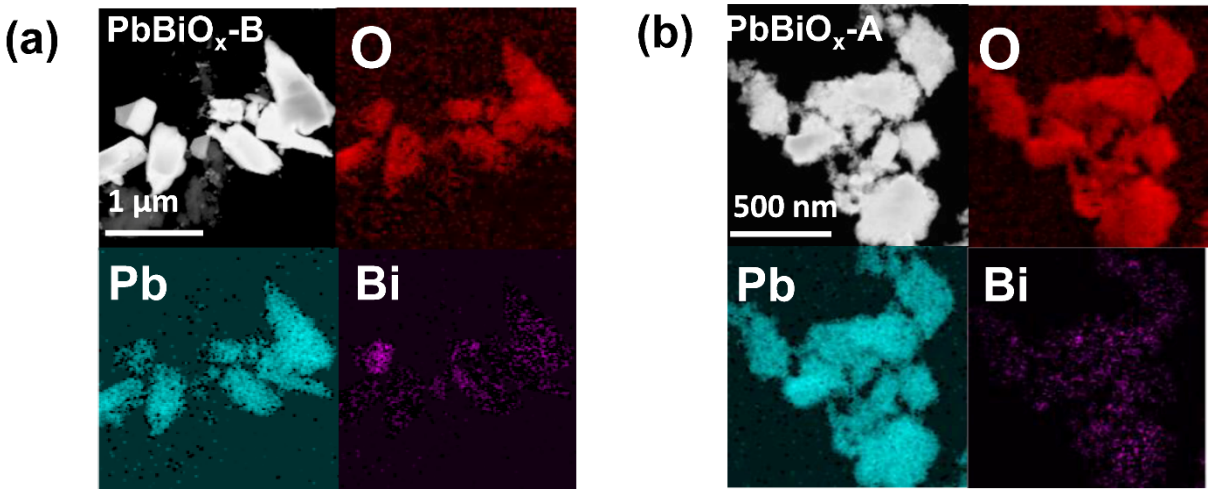

Fig. S19 STEM-EDS mappings of (a) $PbBiO_x$-B and (b) $PbBiO_x$-A.

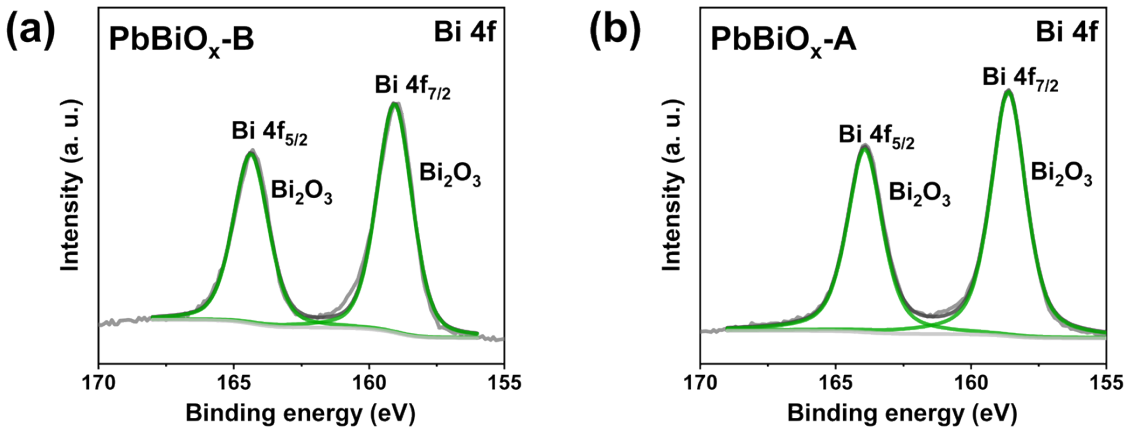

Fig. S20 Bi 4f XPS of (a) $PbBiO_x$-B, and (b) $PbBiO_x$-A

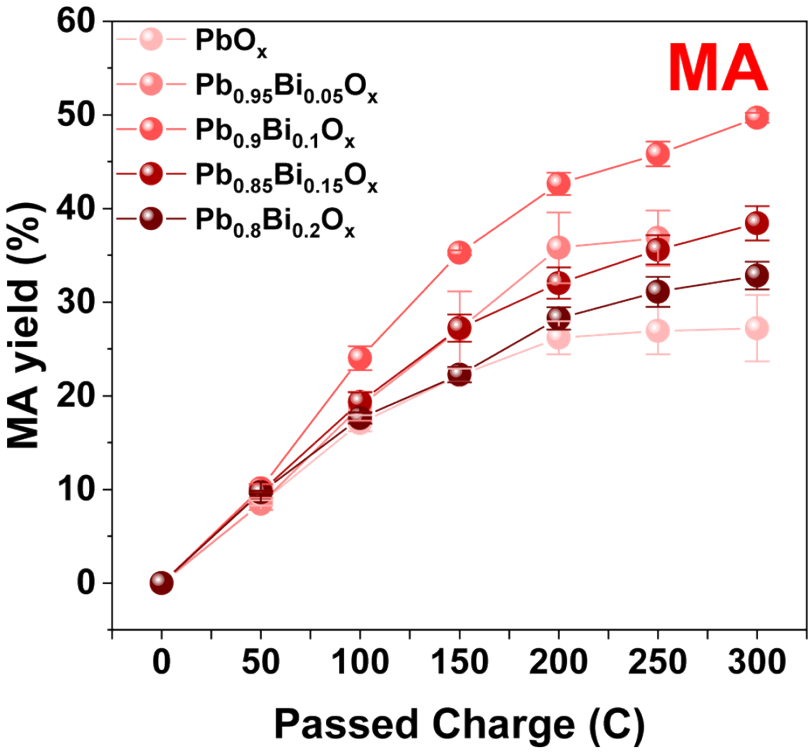

Fig. S21 Graph of MA yield to passed charge.

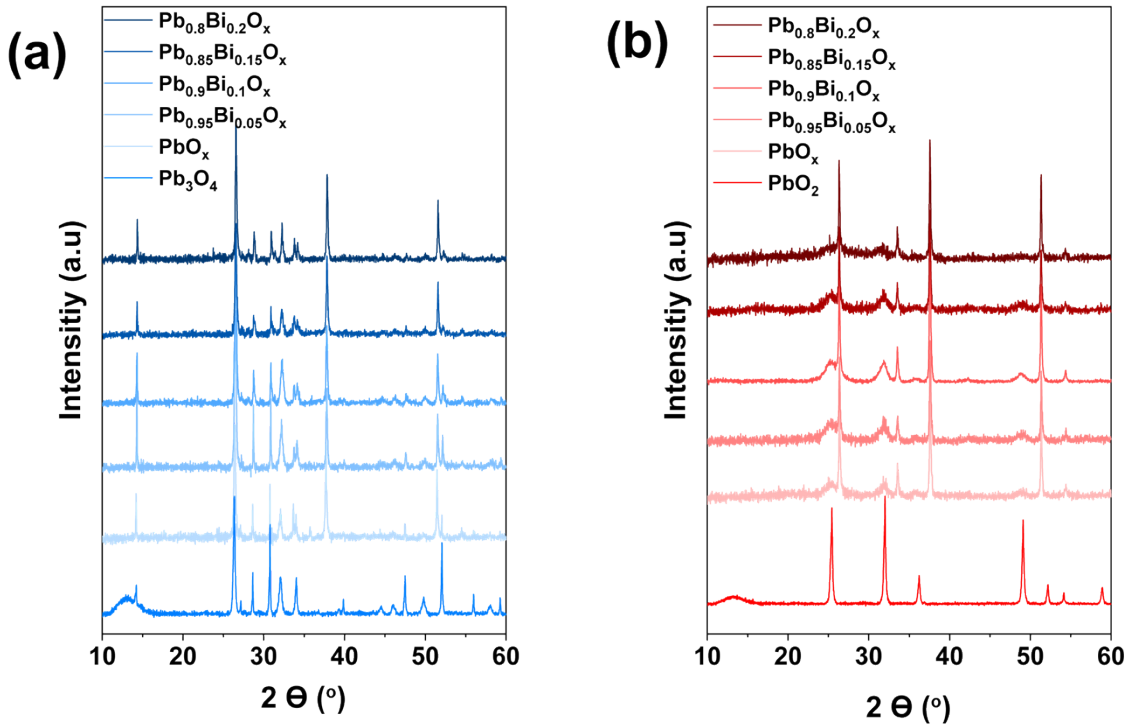

Fig. S22 Overall XRD spectra of $PbBiO_x$ containing different Bi contents of (a) before reaction, and (b) after reaction.

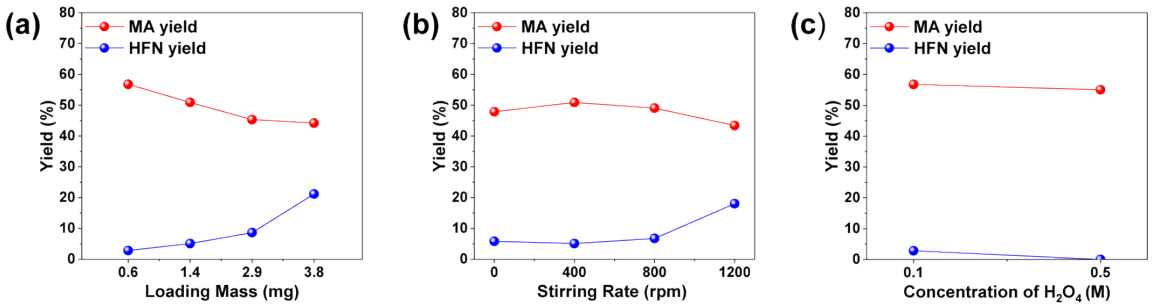

Fig. S23 HFN yield, MA yield trends depending on (a) loading mass, (b) stirring rate, (c) concentrations of H_2SO_4 for electrolyte using $Pb_{0.9}Bi_{0.1}O_x$.

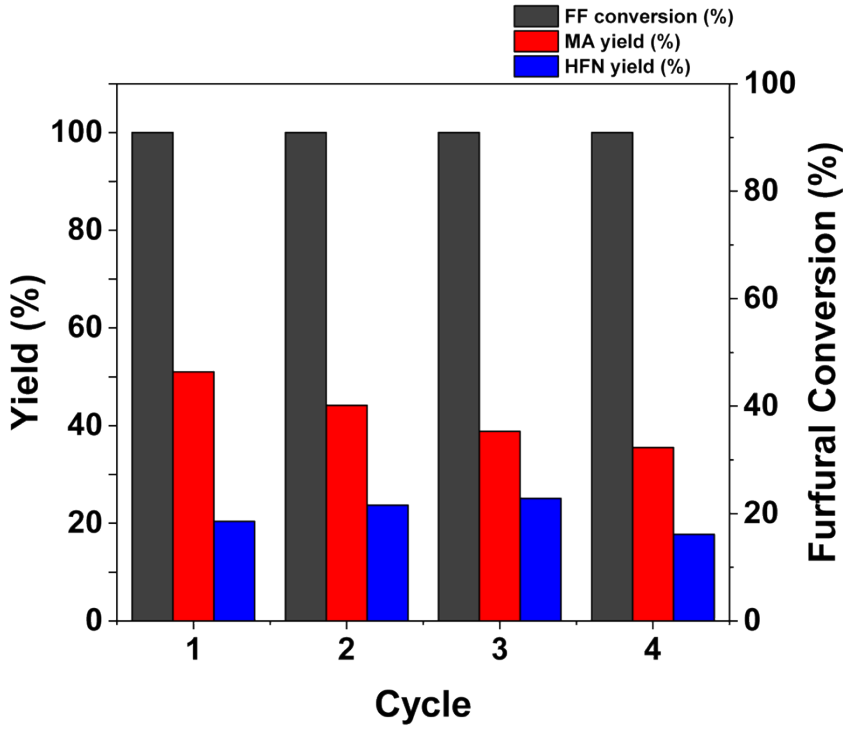

Fig. S24 Cyclic measurement of FFOR using the same $PbBiO_x$ catalyst with 10 mM FF at 2.2 V vs. RHE.

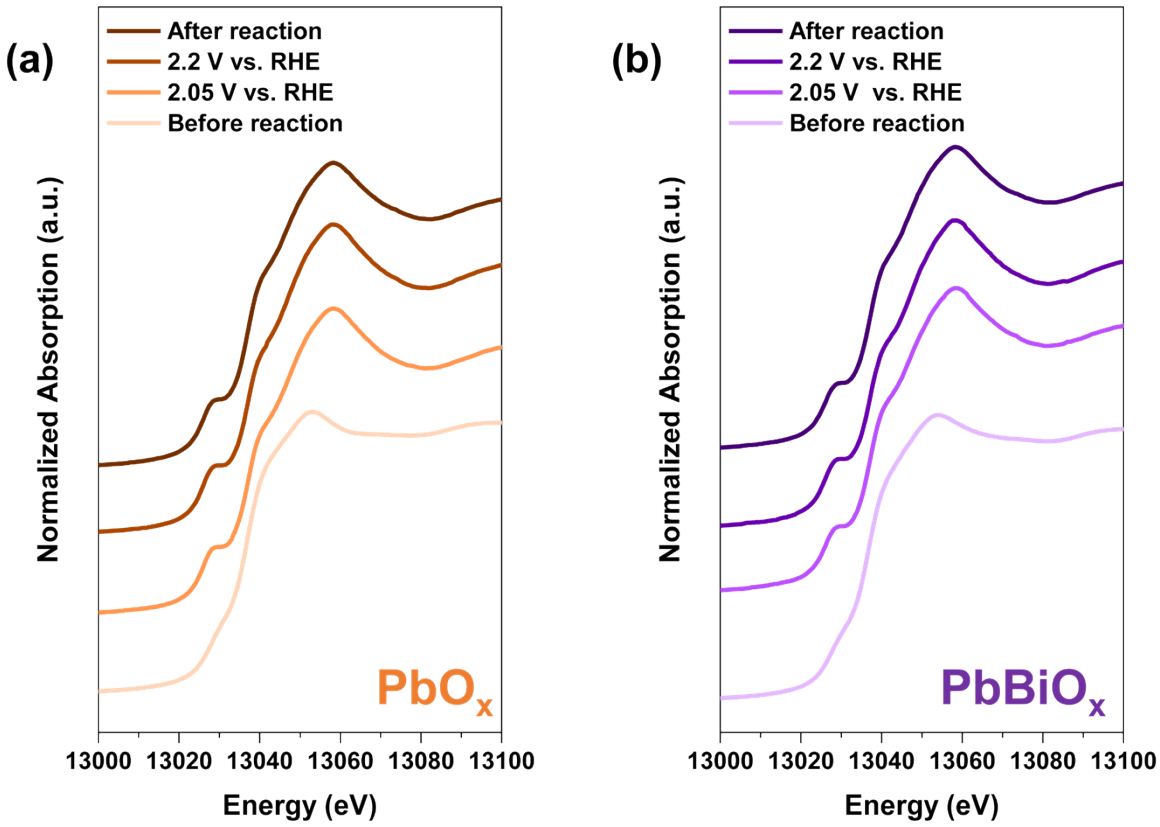

Fig. S25 *Operando* XANES of Pb L_3 of (a) PbO_x, and (b) $PbBiO_x$ under before reaction, 2.05 V vs. RHE, 2.2 V vs. RHE, and after reaction without FF.

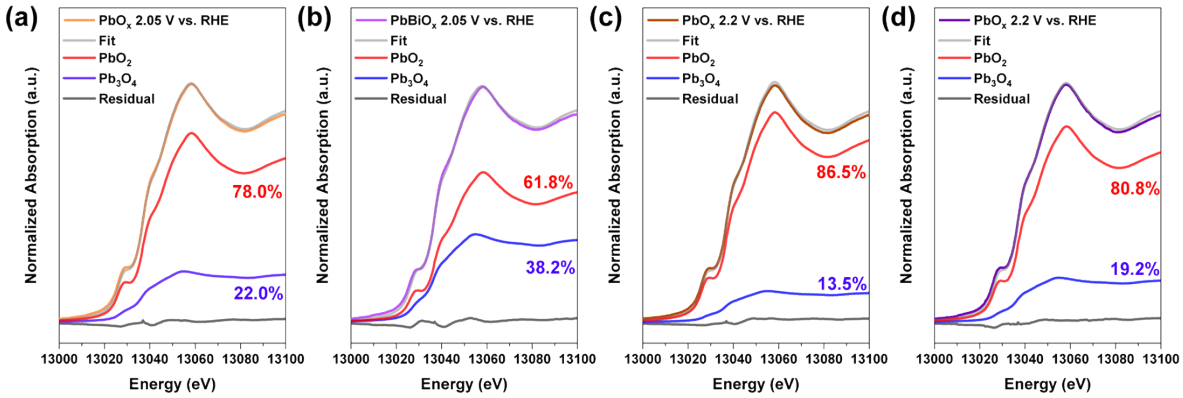

Fig. S26 LCF results of *operando* XANES of (a) PbO_x, (b) $PbBiO_x$ at 2.05 V vs. RHE, (c) PbO_x, and (d) $PbBiO_x$ at 2.2 V vs. RHE.

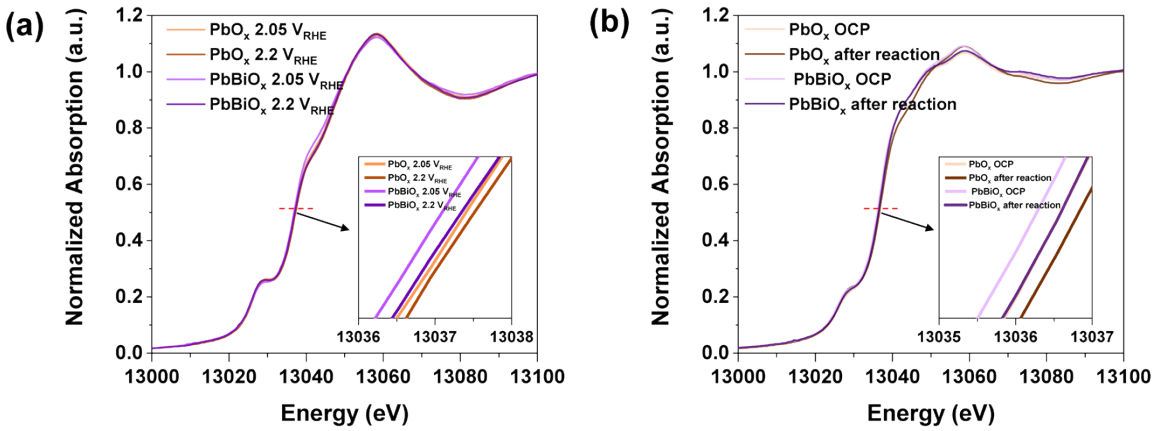

Fig. S27 Overlapped *operando* XANES of Pb L_3 between PbO_x, and $PbBiO_x$ under (a) 2.05 V vs. RHE, and (b) 2.2 V vs. RHE.

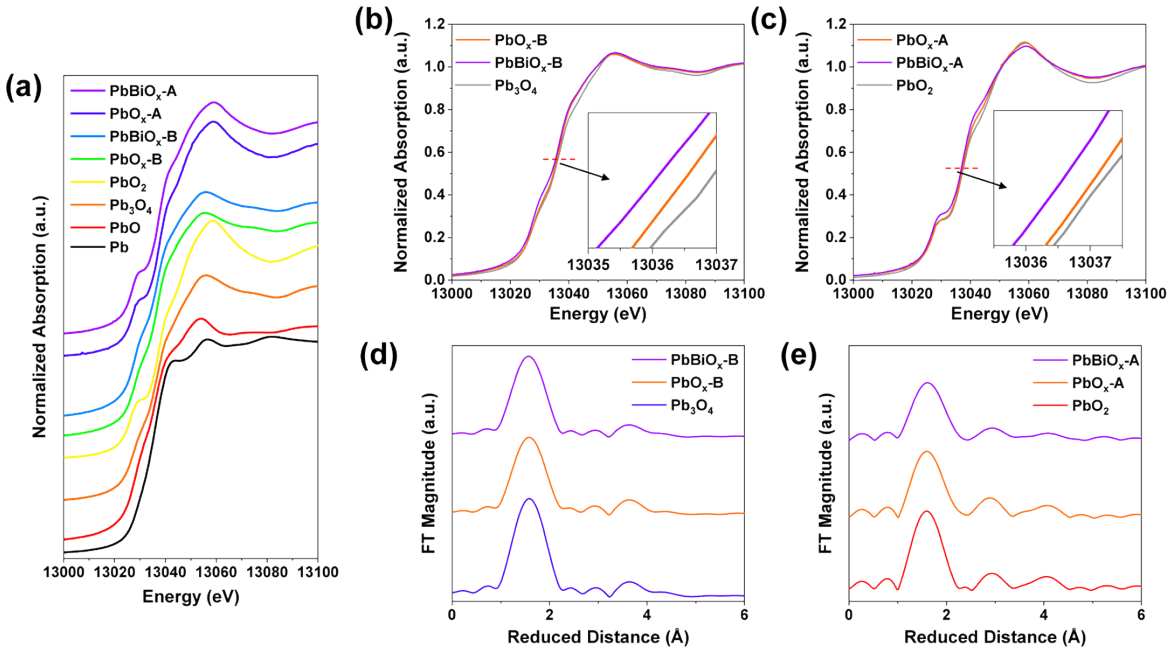

Fig. S28 (a) Overall *ex-situ* Pb L_3 XANES spectra, (b) *ex-situ* XANES spectra of Pb_3O_4, PbO_x-B, and $PbBiO_x$-B. (c) *ex-situ* XANES spectra of PbO_2, PbO_x-A, and $PbBiO_x$-A. (d) *ex-situ* EXAFS of Pb_3O_4, PbO_x-B, and $PbBiO_x$-B. (e) EXAFS of PbO_2, PbO_x-A, and $PbBiO_x$-A.

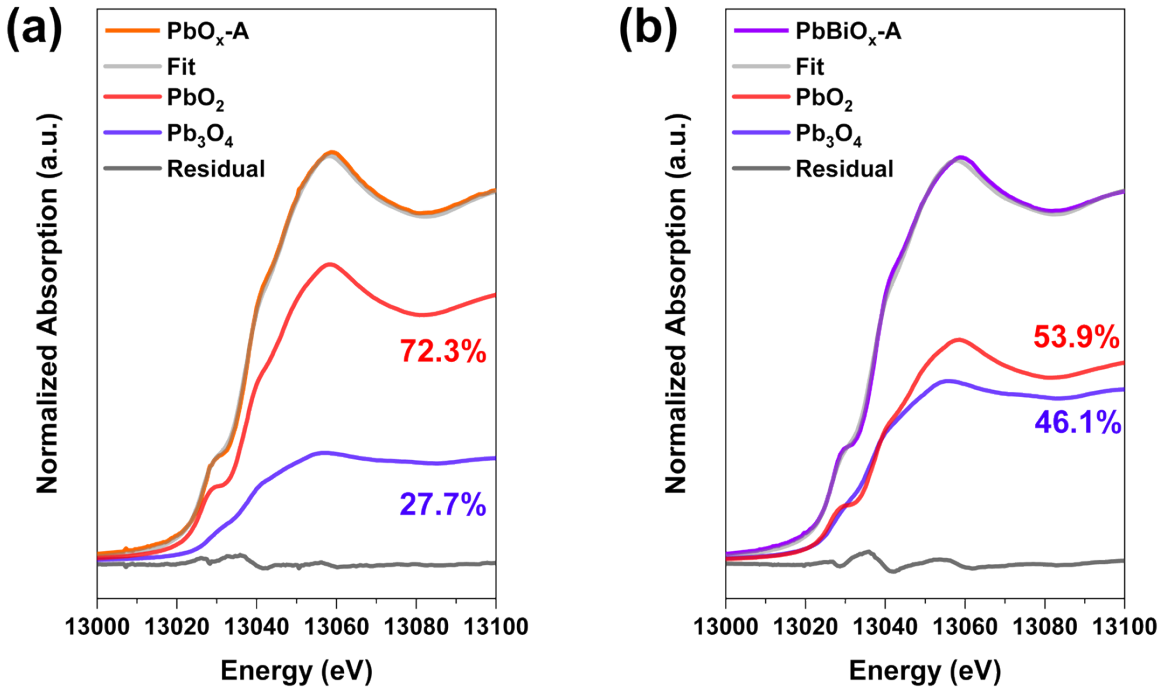

Fig. S29 (a) *ex-situ* LCF results of PbO_x-A, and (b) $PbBiO_x$-A.

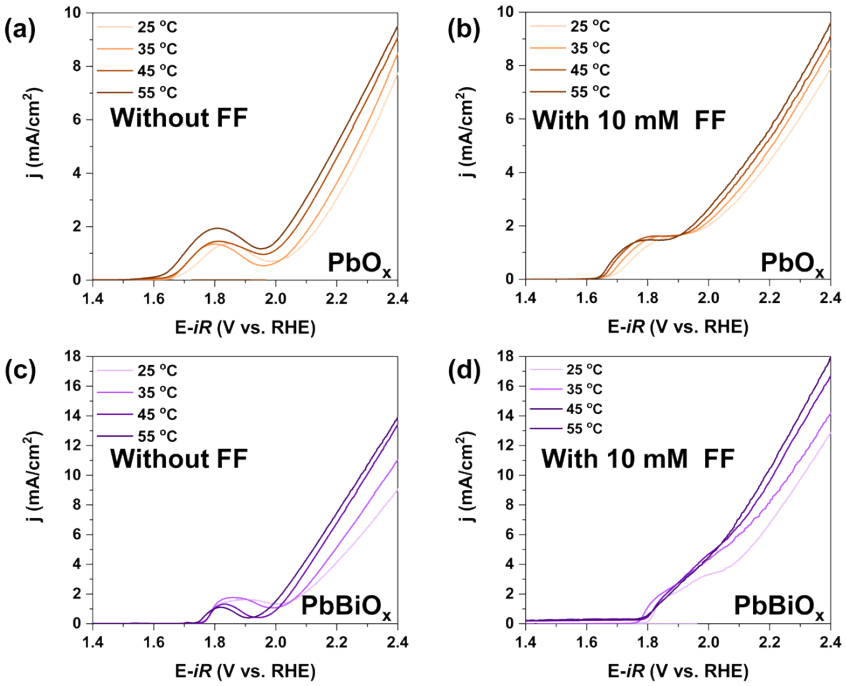

Fig. S30 LSV curves of under different temperature at 25, 35, 45, and 55 ℃ using (a) PbO_x without 10 mM FF, (b) PbO_x with 10 mM FF, (c) $PbBiO_x$ without 10 mM FF, and (d) $PbBiO_x$ with 10 mM FF at a scan rate of 5 mV/s.

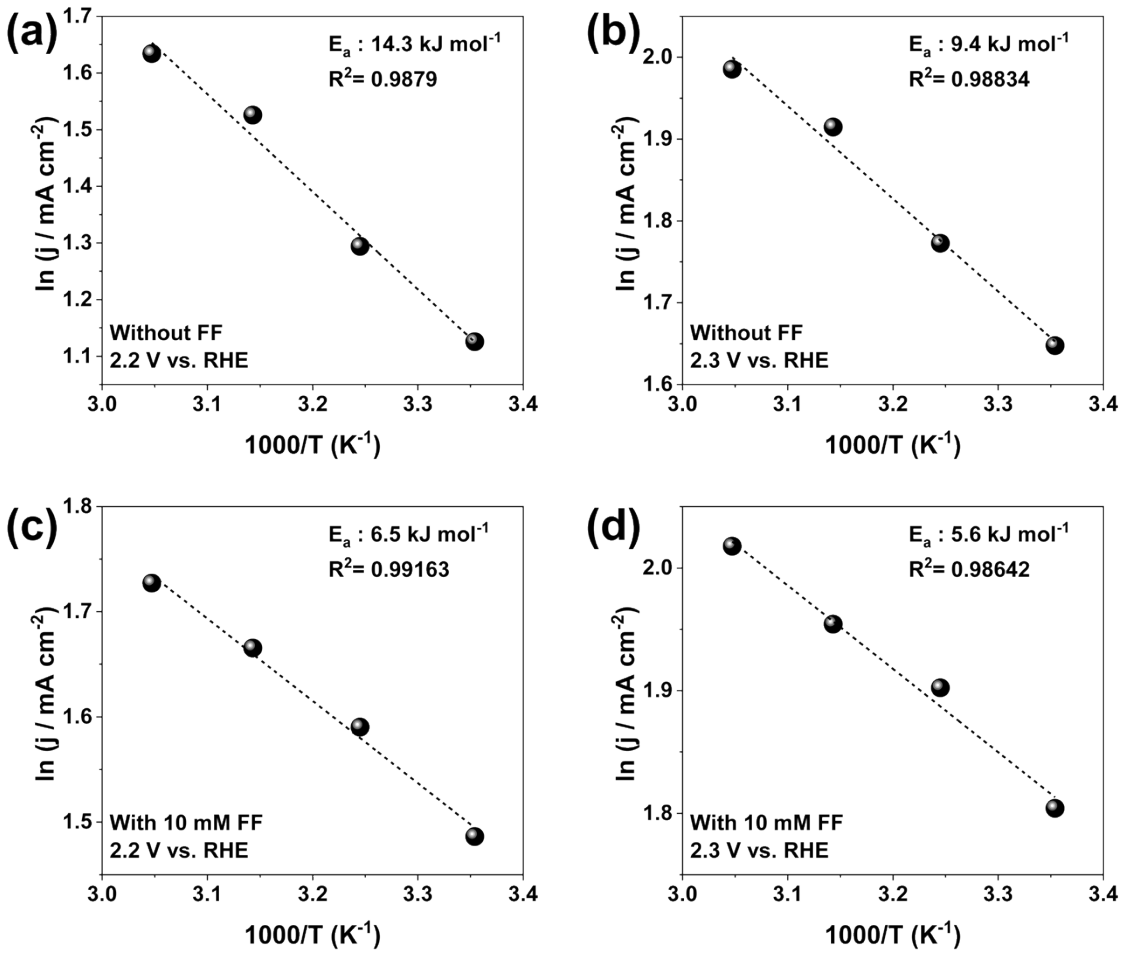

Fig. S31 Activation energy (E_a) of PbO_x in 0.1 M H_2SO_4 at (a) 2.2 V vs. RHE, and (b) 2.3 V vs. RHE, and with 10 mM FF in 0.1 M H_2SO_4 at (c) 2.2 V vs. RHE, and (d) 2.3 V vs. RHE. The E_a value was obtained from slope based on Arrhenius plot of log scale of current densities to reciprocal temperature values.

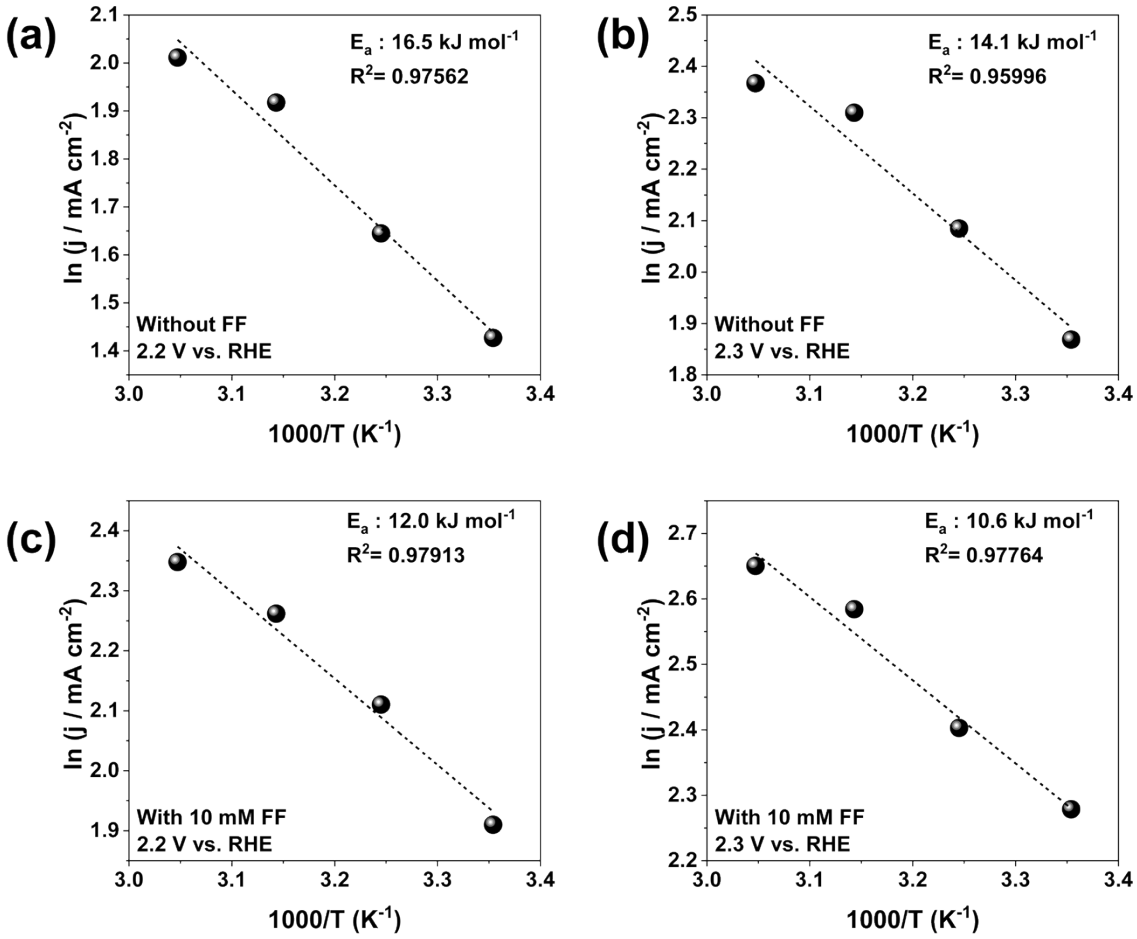

Fig. S32 Activation energy (E_a) of PbO_x in 0.1 M H_2SO_4 at (a) 2.2 V vs. RHE, and (b) 2.3 V vs. RHE, and with 10 mM FF in 0.1 M H_2SO_4 at (c) 2.2 V vs. RHE, and (d) 2.3 V vs. RHE. The E_a value was obtained from slope based on Arrhenius plot of log scale of current densities to reciprocal temperature values.

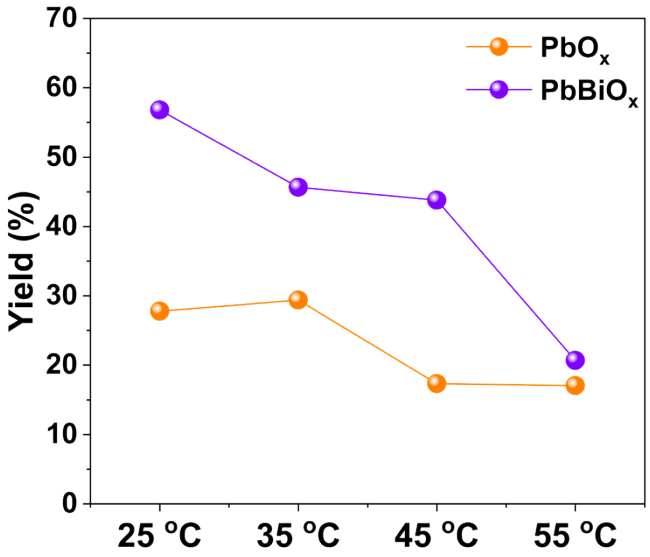

Fig. S33 The FFOR electrolysis results of MA yield using PbO_x, and $PbBiO_x$ at different temperatures under 2.2 V vs. RHE. The orange line is the results of the PbO_x, and the purple line is the results of the $PbBiO_x$.

Table S1 Comparison of the FFOR catalytic performance of $Pb_{0.9}Bi_{0.1}O_x$ with other FFOR system.

	Catalyst	FF Concentration (amount)	Electrolyte (Solvent)	Potential (vs. RHE)	FF Conversion	MA Yield	MA Selectivity in liquids[b]	Additional condition	Ref.
Electrochemical System	$Pb_{0.9}Bi_{0.1}O_x$	10 mM	0.1 M H_2SO_4	2.2 V	100%	57%	90.4%	-	This work
	$Pb_{0.9}Bi_{0.1}O_x$	10 mM	0.5 M H_2SO_4	2.2 V	100%	55%	>99%	-	This work
	ED[a] PbO_x	10 mM	pH 1 H_2SO_4	2.0 V	99%	65.1 %	76.3%	-	1
	Pt/C	100 mM	0.25 M $HClO_4$	1.3 V	-	-	>5%	-	2
	$C_{3.0}N$-$Se_{0.03}$	10 mM	0.5 M $KHCO_3$	1.7 V (vs. Ag/AgCl)	99.5%	84.2 %	84.0% [c]	-	3
Combined System	45 ppi RVC[a], + ACT[a]	50 mM (HFN)	Sodium Buffer[e]	0.8 V (vs. Ag/AgCl)	>99%	89.9 %	92.7%	hv, O_2/ ACT[d]	4
	RVC + EY@NKA[a] + ACT	20 mM	Carbonate buffer[f] /NaOH	0.8 V (vs. A/AgCl)	100%	97%	>99%	hv[g]	5
Thermochemical System	-	1 mmol	HCOOH	-	100%	95%	-	H_2O_2 1 mL[h], 60 °C	6
	TS-1[a]	4.3wt.%	Acetic acid	-	100%	60%	-	80 °C, H_2O_2	7
	-	1 mmol	ChCl-oxalic acid (DES) [a]	-	100%	~30 %	~30%	50 °C H_2O_2 10 mmol	8
	-	>20wt.%	H_2O	-	92%	70%	70%	HFUS[a] 565 kHz, 42 °C	9
	P-C-600[a]	2.5 mmol	H_2O	-	>99%	76.3 %	76.3%[c]	H_2O_2 20 mmol 60 °C	10
	Amberlyst-15	1 mmol	H_2O	-	>99%	11%	13%	H_2O_2 4 mmol	11
	Nb_2O_5	1 mmol	H_2O	-	>99%	5%	15%	H_2O_2 4 mmol	11
	$CaCuP_2O_7$	0.25 g	H_2O	-	~75%	37.4 %	54.8%[c]	115 °C, 0.8 MPa O_2	12
	$H_5PV_2Mo_{10}O_{40}$ •$x$$H_2O$ + $Cu(CF_3SO_2)_2$	2.4 mmol	CH_3CN, acetic acid	-	98.7%	54%	87.8%	20 atm O_2, 110 °C	13
	V_2O_5/γ-Al_2O_3	1vol%	O_2/N_2 (Gas Phase)	-	>99%	~70 %[i]	-	20vol% O_2, 300 °C	14
	$CuMoO_4$/ $Cu(NO_3)_3$	1 mmol	H_2O	-	99%	74%	82%	PMS[a], 2 MPa air, 140 °C	15

[a] Acronyms: ED: electrodeposited, RVC: reticulated vitreous carbon, ACT: 4-acetamido-2,2,6,6-tetramethylpiperidine-1-oxyl, EY@NKA: resin-supported Eosin Y (photo-oxygenation) DES: deep eutectic solvent, TS-1: titanium silicate-1, HFUS: high frequency ultrasound, P-C-600: pyrolysis of phytic acid at 600 °C annealing temperature, PMS: peroxymonosylfate.

[b] selectivity of liquid products: $$Selectivity\ in\ liquid\ products\ (\%) = \frac{yield\ of\ certain\ product}{yield\ of\ all\ liquid\ products} \times 100$$

[c] selectivity products: $$Selectivity\ of\ products\ (\%) = \frac{yield\ of\ certain\ product}{yield\ of\ all\ liquid\ products} \times 100$$

[d] The production of MA was conducted via two step reaction. The reaction from FF to HFN occurred via photochemical oxidation in methanol solvent with photochemically generated singlet oxygen as oxidant and ACT-mediated electrocatalytic reaction from HFN to FF was operated.

[e] 0.34 M Na_2CO_3 + 0.06 M $NaHCO_3$ as anolyte, NaOH as catholyte.

[f] 0.34 M Na_2CO_3 + 0.06 M $NaHCO_3$ (pH 8.5).

[g] ACT-mediated photoelectrocatalytic reaction using EY@NKA as photo-oxygenation under irradiation by LEDs.

[h] 3.5-fold amount of H_2O_2 volume than FF.

[i] Maleic anhydride which converted to maleic acid in aqueous solution.

Table S2 Results of FFOR depending on different electrolyte (pH).

Electrolyte (pH)	FF Conversion (%)	MA Yield (%)	HFN Yield (%)	HFA Yield (%)	FA Yield (%)	Applied Potential (vs. RHE)	Passed Charge (C)
0.1 M H_2SO_4 (pH 1)	100	26.9%	25.3	0	1.4	2.2	250
0.1 M $NaHPO_4/Na_2PO_4$ (pH 6.77)	100	16.4%	45.6%	-	16.0%	2.4	250
0.1 M KOH[a] (pH 13)	75.3%	9.1%	-	-	-	2.4	135

[a] Other intermediate species were not detected due to degradation of organic species in alkaline media.

Table S3 FFOR results of PbO_x at 2.2 V vs. RHE.

Passed Charge (C)	FF Conversion (%)	MA Yield (%)	HFN Yield (%)	HFA Yield (%)	FA Yield (%)	Loss (%)	F.E (%)
50	72.4	8.5	26.8	7.3	12.8	29.8	72.0
100	96.5	17	41.7	7.0	11.1	33.0	58.9
150	100	22.2	41.3	1.5	5.4	35.0	40.1
200	100	26.2	34.8	0	2.5	39.0	29.3
250	100	26.9	25.3	0	1.4	47.8	20.6
300	100	27.2	22.1	0	1.5	50.6	16.5

Table S4 FFOR results of $Pb_{0.95}Bi_{0.05}O_x$ at 2.2 V vs. RHE.

Passed Charge (C)	FF Conversion (%)	MA Yield (%)	HFN Yield (%)	HFA Yield (%)	FA Yield (%)	Loss (%)	F.E (%)
50	64.6	10.1	34.7	1.5	28.5	18.3	90.6
100	93.6	24.0	47.3	2.0	18.9	20.4	74.2
150	100	35.3	33.2	0	10.7	31.5	49.3
200	100	42.6	18.8	0	2.7	38.6	34.8
250	100	45.8	11.5	0	2.0	42.6	26.8
300	100	50.0	8.1	0	1.1	42.2	22.9

Table S5 FFOR results of $Pb_{0.95}Bi_{0.05}O_x$ at 2.2 V vs. RHE.

Passed Charge (C)	FF Conversion (%)	MA Yield (%)	HFN Yield (%)	HFA Yield (%)	FA Yield (%)	Loss (%)	F.E (%)
50	71.5	0	28.2	6.3	18.7	28.6	89.4
100	96.8	8.4	47.5	5.0	17.9	35.4	57.6
150	100	18.9	28.1	0.8	6.0	44.0	42.1
200	100	35.8	20.9	0	3.3	43.2	31.1

250	100	36.8	14.0	0	2.0	49.2	23.0

Table S6 FFOR results of $Pb_{0.85}Bi_{0.15}O_x$ at 2.2 V vs. RHE.

Passed Charge (C)	FF Conversion (%)	MA Yield (%)	HFN Yield (%)	HFA Yield (%)	FA Yield (%)	Loss (%)	F.E (%)
50	66.2	9.7	29.5	2.7	23.5	24.2	84.7
100	91.2	19.3	43.1	2.7	27.3	36.0	67.7
150	99.7	27.2	41.7	0.4	16.1	30.4	49.9
200	100	32.0	35.1	0	7.1	32.8	37.3
250	100	35.6	26.6	0	4.9	37.8	28.4
300	100	38.4	21.5	0	2.3	40.1	23.2

Table S7 FFOR results of $Pb_{0.8}Bi_{0.2}O_x$ at 2.2 V vs. RHE.

Passed Charge	FF Conversion (%)	MA Yield (%)	HFN Yield (%)	HFA Yield (%)	FA Yield (%)	Loss (%)	F.E (%)
50	70.2	9.7	35.6	3.5	31.2	21.4	91.5
100	96.0	17.6	47.3	2.6	23.6	28.4	67.9
150	100	22.3	42.8	0	20.4	34.9	45.5
200	100	28.3	42.3	0	14.9	29.4	37.2
250	100	31.1	35.4	0	9.0	33.5	28.7
300	100	32.8	28.5	0	5.7	38.6	22.4

Table S8 The Bi and Pb ratio of $PbBiO_x$ based on EDS mapping.

Sample Name	Contents (atomic %)				Bi/Pb (%)
	Pb	Bi	O	Sn	
$Pb_{0.95}Bi_{0.05}O_x$	19.46	1.15	64.75	14.64	5.91
$Pb_{0.9}Bi_{0.1}O_x$	18.90	1.91	66.68	12.51	10.11
$Pb_{0.85}Bi_{0.15}O_x$	8.50	1.36	68.56	21.58	16.00
$Pb_{0.8}Bi_{0.2}O_x$	15.09	3.65	65.31	15.94	24.19

References

1. S. R. Kubota and K.-S. Choi, *ACS Sustainable Chem. Eng.*, 2018, **6**, 9596-9600.
2. A. M. Román, J. C. Hasse, J. W. Medlin and A. Holewinski, *ACS Catal.*, 2019, **9**, 10305-10316.
3. X. Huang, J. Song, M. Hua, B. Chen, Z. Xie, H. Liu, Z. Zhang, Q. Meng and B. Han, *Chem. Sci.*, 2021, **12**, 6342-6349.
4. S. Thiyagarajan, D. Franciolus, R. J. Bisselink, T. A. Ewing, C. G. Boeriu and J. Van Haveren, *ACS Sustainable Chem. Eng.*, 2020, **8**, 10626-10632.
5. G.-H. Lu, M.-H. Zong and N. Li, *ACS Catal.*, 2023, **13**, 1371-1380.
6. X. Li, B. Ho, D. S. W. Lim and Y. Zhang, *Green Chem.*, 2017, **19**, 914-918.
7. Y. Lou, S. Marinkovic, B. Estrine, W. Qiang and G. r. Enderlin, *ACS Omega*, 2020, **5**, 2561-2568.
8. Y. Ni, Z. Bi, H. Su and L. Yan, *Green Chem.*, 2019, **21**, 1075-1079.
9. N. Ayoub, J. Toufaily, E. Guénin and G. Enderlin, *Green Chem.*, 2022, **24**, 4164-4173.
10. H. Zhang, S. Wang, H. Zhang, J. H. Clark and F. Cao, *Green Chem.*, 2021, **23**, 1370-1381.
11. H. Choudhary, S. Nishimura, and K. Ebitani, *Appl. Catal. A*, 2013, **458**, 55-62.
12. T. Soták, M. Hronec, M. Gál, E. Dobročka and J. Škriniarová, *Catal. Lett.*, 2017, **147**, 2714-2723.
13. J. Lan, Z. Chen, J. Lin and G. Yin, *Green Chem.*, 2014, **16**, 4351-4358.
14. N. Alonso-Fagúndez, M. Ojeda, R. Mariscal, J. L. G. Fierro and M. López Granados, *J. Catal.*, 2017, **348**, 265-275.
15. X. Yu, H. Liu, Q. Wang, W. Jia, H. Wang, W. Li, J. Zheng, Y. Sun, X. Tang, X. Zeng, F. Xu and L. Lin *ACS Sustainable Chem. Eng.*, 2021, **9**, 13176-13187.